

Article

Numerical Simulation of a Novel Method for PVT Growth of SiC by Adding a Graphite Block

Hao Luo ¹, Xuefeng Han ^{2,*} , Yuanchao Huang ^{1,2}, Deren Yang ^{1,2} and Xiaodong Pi ^{1,2,*}

¹ State Key Laboratory of Silicon Materials and School of Materials Science and Engineering, Zhejiang University, Hangzhou 310027, China; 21926067@zju.edu.cn (H.L.); huangyuanchao@zju.edu.cn (Y.H.); mseyang@zju.edu.cn (D.Y.)

² Hangzhou Global Scientific and Technological Innovation Center, Zhejiang University, Hangzhou 311200, China

* Correspondence: xuefenghan@zju.edu.cn (X.H.); xdpi@zju.edu.cn (X.P.)

Abstract: SiC crystal is an excellent substrate material for high power electronic devices and high-frequency electronic devices. Being cost-effective and defect-free are the two biggest challenges at present. For the physical vapor transport (PVT) growth of a SiC single crystal, SiC powder is used as the source material, which determines the cost and the quality of the crystal. In this paper, we propose a new design in which graphite blocks are substituted for the non-sublimated SiC powder. Temperature distribution in the SiC powder, the evolution of the SiC powder, and the vapor transport are investigated by using finite element calculations. With the addition of graphite blocks, the utilization and sublimation rate of SiC powder is higher. In addition, the reverse vapor transport above the SiC powder is eliminated. This design provides a new idea to reduce the cost of SiC crystals in industrialization.

Keywords: simulation; powder evolution; gas transport; graphite block; SiC crystal



Citation: Luo, H.; Han, X.; Huang, Y.; Yang, D.; Pi, X. Numerical Simulation of a Novel Method for PVT Growth of SiC by Adding a Graphite Block. *Crystals* **2021**, *11*, 1581. <https://doi.org/10.3390/cryst11121581>

Academic Editors: Haiding Sun, Bharat Jalan, Shibing Long, Yuhao Zhang, Rajendra Singh, Xuelin Yang, Yuji Zhao and Bin Liu

Received: 13 November 2021
Accepted: 16 December 2021
Published: 18 December 2021

Publisher's Note: MDPI stays neutral with regard to jurisdictional claims in published maps and institutional affiliations.



Copyright: © 2021 by the authors. Licensee MDPI, Basel, Switzerland. This article is an open access article distributed under the terms and conditions of the Creative Commons Attribution (CC BY) license (<https://creativecommons.org/licenses/by/4.0/>).

1. Introduction

As one of the most important third-generation semiconductor materials, SiC has received widespread attention due to its wide band gap, high breakdown field strength, high thermal conductivity, and high carrier saturation mobility [1–4]. Devices based on SiC substrate have been widely used in important fields such as electrical vehicles and 5G communication [5,6]. Physical vapor transport (PVT) is the main method for growing a large-size SiC single crystal, which needs to be cost-effective and defect-free.

SiC powder is used as the source material during the PVT growth of a SiC single crystal [7]. The utilization rate and sublimation process of SiC powder directly affect the crystal quality and fabrication cost of SiC. Previous studies used in situ X-ray technology to analyze the evolution of the source material during the crystal growth [8–12]. Researchers also established a crystal growth model to study the effect of the temperature, temperature gradient, and the particle size of SiC powder on the sublimation of SiC powder and the growth of a SiC single crystal [13–15]. Wang et al. found that the sublimation of SiC powder was insufficient, and they increased the crystal growth rate by the optimization of powder packaging [16]. Li et al. studied the sublimation process of SiC powder in a traditional structure by the finite element method and found that the sublimation rate of SiC powder can be improved by adjusting the coil height [17]. However, there are few research works on the relationship between the graphite structure design and the utilization rate of SiC powder [18].

In this work, we propose a new powder composition, in which part of the SiC powder is replaced with a graphite block. The utilization rate of SiC powder is improved, reducing the cost of SiC crystal growth. Moreover, the excellent thermal conductivity of graphite optimizes the vapor transport above the powder helping to improve the crystal quality.

2. Materials and Methods

The finite element method enabled by the software of Virtual Reactor 6.5 was employed to investigate the SiC crystal growth. This software can accurately assign values to the crystal growth process, and the simulation results are close to the actual values [14,19]. Figure 1a is a 2D axis-symmetric global model for the PVT growth of a SiC single crystal. This is an induction heating system. The outer layer of the system is an induction coil, and the inner part is a graphite crucible wrapped by graphite felt, in which the crystal is grown. Figure 1b is the meshing of the model for finite element calculation. The calculation domain of powder is made of structured mesh with a side length of 2 mm, and the other domains are unstructured mesh. During the PVT process, the seed crystal temperature is 2100 °C. The pressure is 500 Pa. The growth time is 50 h.

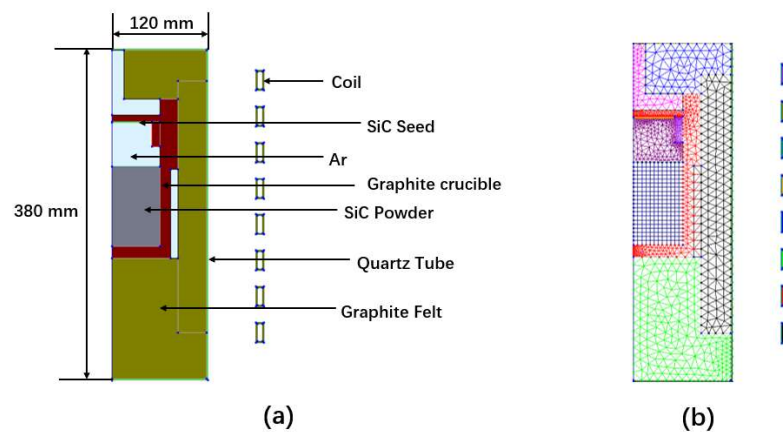


Figure 1. Crystal growth system in finite element calculations: (a) global model for the PVT growth of SiC single crystal. (b) the meshing of the calculation model.

In this paper, we focus on the SiC powder inside of the graphite crucible. In a traditional process (Figure 2a), the seed crystal and SiC powder are placed in a graphite crucible. The SiC powder is stacked at the bottom of the graphite crucible, while the SiC seed crystal is placed on the top of the graphite crucible. Gas derived from the sublimation of the SiC powder is transported to the surface of the seed crystal. However, previous studies found that the difference in temperature in the SiC powder is too large, resulting in excessive local sublimation of powder and a low utilization rate [17]. To improve the utilization rate of powder, we propose a model with a new design of the powder (Figure 2b) and investigate the temperature distribution in the SiC powder, the evolution of the SiC powder, and the gas transport.

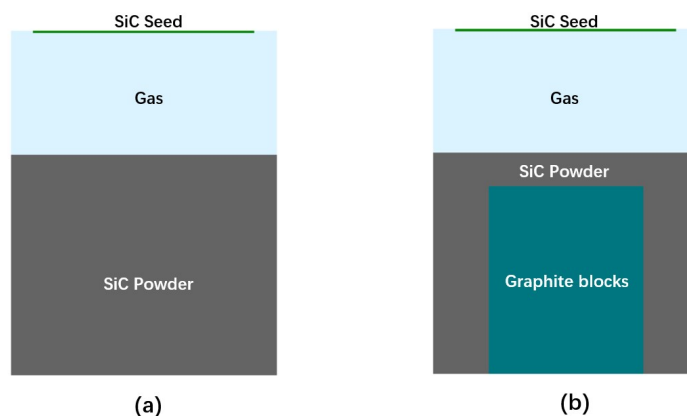


Figure 2. Different structures inside the graphite crucible: (a) traditional structure. (b) optimized structure.

The global heat transfer includes heat conduction in solid media, heat conduction and convection in the gas, and radiation heat exchange in gas between solid surfaces. The heat conduction is described by the following equations:

$$\rho C_P \frac{\partial T}{\partial t} + \rho C_P u \nabla T + \nabla \cdot q = Q \quad (1)$$

$$q = -k \nabla T \quad (2)$$

where ρ is the density, C_P is the thermal capacity, u is the velocity, T is the temperature, q is the local heat flux, and k is the thermal conductivity.

The heat flux of the boundary conditions is calculated as:

$$q_w = \lambda \frac{T_w - T_c}{dx} \quad (3)$$

where λ is the thermal conductivity of the wall, T_w is the wall temperature, and T_c is cell center temperature.

In the boundary conditions of the heat exchange walls, the radiative heat flux at the wall is calculated as:

$$q_w = \sigma \epsilon_w (T_a^4 - T_w^4) \quad (4)$$

where T_a is the ambient temperature, T_w is the wall temperature, σ is the Stefan-Boltzmann constant, and ϵ_w is the wall emissivity.

The evolution of the powder and species transport in the porous source is also calculated. SiC powder is considered as a porous medium by local porosity, granule size, and graphitization degree. The powder porosity is defined as:

$$\varepsilon = \frac{V_f}{V_{cell}} \quad (5)$$

where V_{cell} is the total volume of the computational cell, and V_f is the volume of the fluid fraction of the cell.

Species transport in the powder is described by the Darcy-Brinkman-Forchheimer (DBF) flow model. The continuity equations for the whole vapor and for each species are as follows:

$$\frac{\partial \rho}{\partial t} + \nabla \cdot (\rho \vec{V}) = S^m \quad (6)$$

where \vec{V} is flow velocity inside the pores, and S^m is the mass source. Flow in the porous medium is described by the DBF equations as follows:

$$\frac{\rho}{\varepsilon} \frac{\partial \vec{V}}{\partial t} + \frac{1}{\varepsilon} \nabla \cdot \left(\frac{1}{\varepsilon} \rho \vec{V} \vec{V} \right) = -\nabla p - \frac{\mu}{K} \vec{V} + \nabla \cdot \tau - \frac{\rho C_F}{\sqrt{K}} \left| \vec{V} \right| \vec{V} - \rho \vec{g} \quad (7)$$

$$\tau = 2\mu \dot{S} - \frac{2}{3}\mu \left(\nabla \cdot \vec{V} \right) I \quad (8)$$

where ε is powder porosity, p is the gas pressure, μ is the gas viscosity, K is the powder permeability, C_F is the inertial coefficient, τ is the stress tensor, g is the gravitational acceleration, and I is the tensor unity.

The boundary conditions for the above set of equations at all reaction boundaries of the powder can be written as:

$$V_n = V_{stef} \quad (9)$$

$$V_\tau = 0 \quad (10)$$

where V_{stef} is the Stefan velocity and V_n and V_τ are normal velocity and tangential velocity.

For the non-reaction boundaries:

$$\vec{V} = 0 \quad (11)$$

The values that appear in the above formula can be found in the Table 1.

Table 1. Major physical properties and operating parameters in the model.

Properties	Value and Unit
Density of graphite crucible	1730 kg/m ³
Density of insulation layer	200 kg/m ³
Density of seed crystal	3220 kg/m ³
Heat capacity of graphite crucible	2250 J/(kg·K)
Heat capacity of insulation layer	1000 J/(kg·K)
Heat capacity of seed crystal	1281 J/(kg·K)
Thermal conductivity of graphite crucible	$22.3 + (2.3 \times 10^7)/(1 + (T/0.00056))$ W/(m·K)
Thermal conductivity of insulation layer	$0.08 \exp(0.00117 \exp(T - 300))$ W/(m·K)
Thermal conductivity of seed crystal	$288 (T/300) - 1.29$ W/(m·K)
Gas viscosity	8×10^{-5} Pa·s
Emissivity of wall	0.8
Emissivity of graphite crucible	0.8
Emissivity of insulation layer	0.8
Emissivity of seed crystal	0.9
Powder porosity	0.6
Powder permeability	0.8

3. Results and Discussion

Figure 3a,b shows the heat flux in different structures. The added graphite block increased the heat flux of the powder in the top area by thermal contact. Figure 3c,d shows the temperature distributions in the SiC powder for different structures. In both structures, the highest temperature area was at the bottom corner of the graphite crucible, and the lowest temperature area was at the top surface of the SiC powder. However, it was different for the temperature gradient at the powder surface. As shown in Figure 3e, for the optimized powder, the radial temperature was higher, and the temperature difference was smaller. Figure 3f shows the axial temperature gradient. The temperature in the centerline (line C-A) increased greatly compared to the traditional one. From the above results, we conclude that the temperature distribution of powder surface is more uniform by adding the graphite block.

Figure 4 shows the porosity change of the powder after crystal growth for 50 h in different structures. We defined the porosity of the SiC powder as 0.6 before growth. In the process of crystal growth, the porosity of SiC powder increased after sublimation and decreased after recrystallization. Therefore, the evolution of SiC powder during growth can be investigated by the change in porosity. In the traditional structure (Figure 4a), we find that only the powder close to the crucible wall sublimated, the powder at the top and bottom of the powder recrystallized, and the powder in the middle part was basically unchanged. This means that the utilization rate of the SiC powder in the traditional structure was very low. In the optimized structure, we used graphite block instead of SiC powder, which did not participate in the reaction. As can be seen from Figure 4b, the powder above the graphite block also sublimated, and the powder that did not participate in the reaction was greatly reduced.

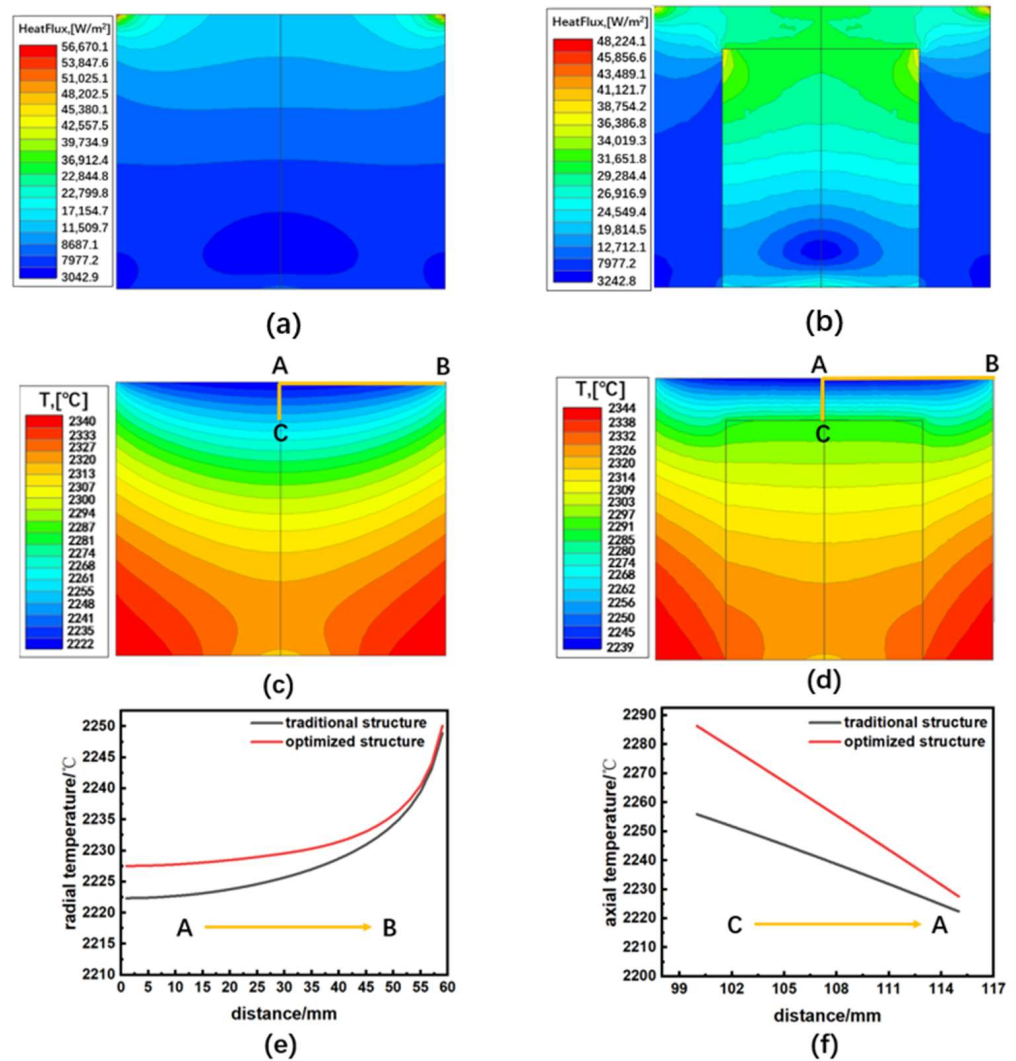


Figure 3. The thermal field in the SiC powder: (a) the heat flux in the traditional structure, (b) the heat flux in the optimized structure, (c) the temperature distribution in the traditional structure, (d) the temperature distribution in the optimized structure, (e) the radial temperature gradient, and (f) the axial temperature gradient.

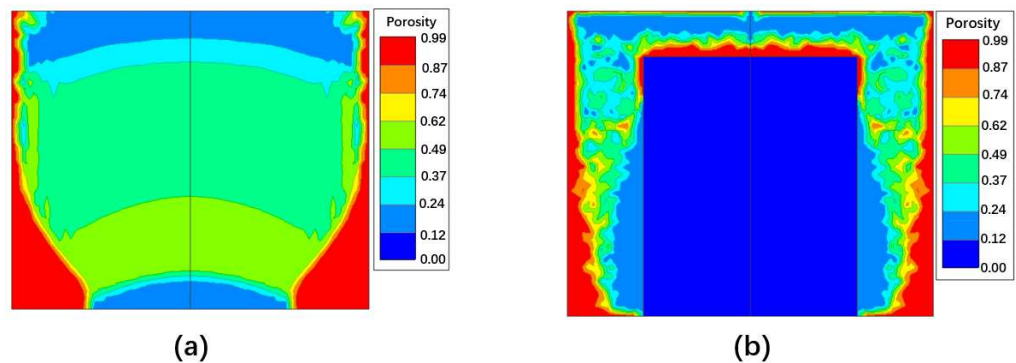


Figure 4. The porosity changes of powder after crystal growth for 50 h in different structures: (a) in the traditional structure and (b) in the optimized structure.

In the process of crystal growth, the sublimation rate of powder will directly affect the concentration of reaction gas. The non-stoichiometric decomposition products of the SiC powder are mainly SiC₂ and Si₂C. We kept the pressure in the growth chamber constant at

500 Pa and calculated the pressure fraction of the SiC_2 and Si_2C gas on the surface of the seed crystal with the increase in growth time. Figure 5 shows that during the whole growth process, the pressure fraction of SiC_2 and Si_2C in the optimized structure were higher than those in the traditional structure, indicating that the sublimation rate of SiC powder in the optimized structure was higher.

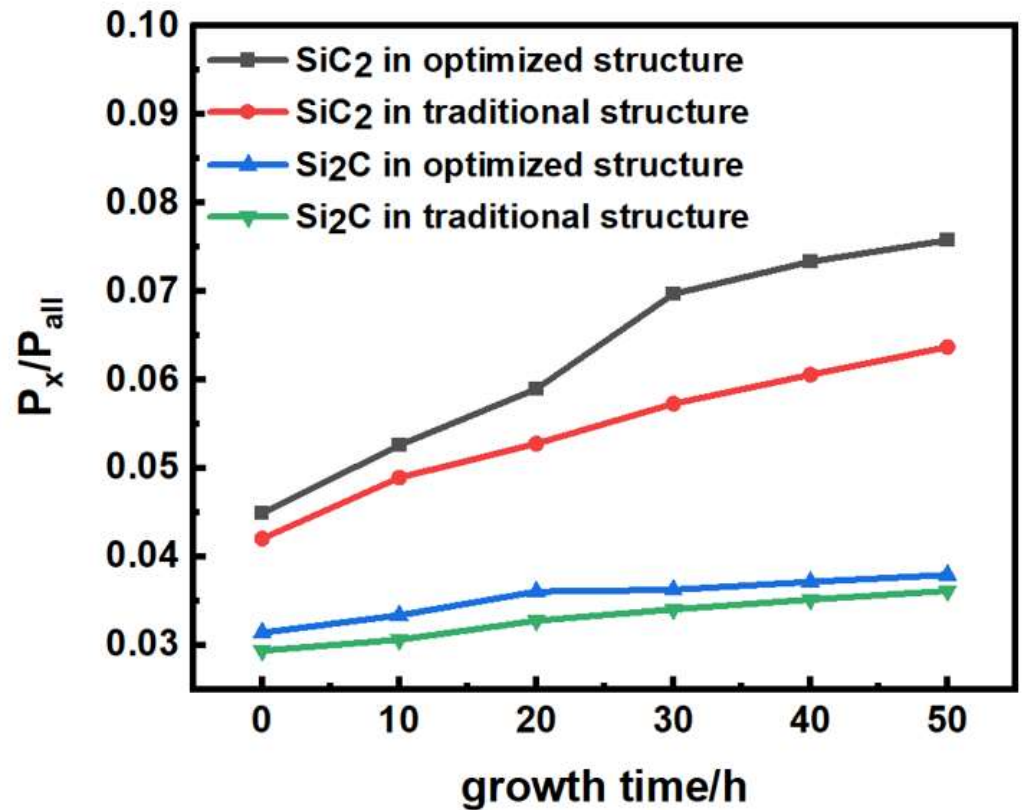


Figure 5. The pressure fraction of SiC_2 and Si_2C gas in different structures.

In order to explore the influence of temperature and powder evolution on the gas transport, we investigated the gas transport process in different structures. Figure 6a shows the flow path of the sublimated SiC (Si , Si_2C , SiC_2) during the growth process. In the traditional structure, the vapor in the powder flowed out close to the crucible wall. Part of the vapor reached the surface of the seed crystal. The rest flowed in the reverse direction. We believe that the reverse transport was caused by the evolution difference between the surface powder and the bottom powder. The low temperature of the powder on the surface led to low vapor saturation, and the vapor transport from the high temperature on both sides recrystallized on the surface, forming the reverse transport. The reverse transport not only caused gas turbulence in the growth area but also prevented internal gas from flowing out of the central area. Yang [20] studied the carbon inclusions in PVT-grown SiC single crystal. They pointed out that carbon inclusions were induced by the graphitization of raw materials. Our current results show that vapor could only be transported from the highly graphitized powder because of the reverse transport, which undoubtedly increased the possibility of carbon inclusion.

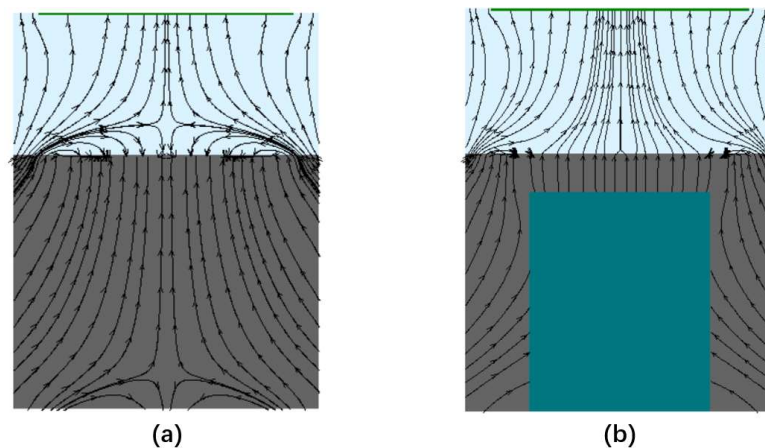


Figure 6. Gas flow field: (a) in the traditional structure model and (b) in the optimized structure model.

Figure 6b shows the gas transport in the optimized structure. After the graphite block was added, there was no longer reverse transport above the powder, and the gas in the powder flowed uniformly and in the same direction when it flowed to the surface of the seed crystal. We believe that the graphite blocks raised the temperature of the surface powder, and the powder on the surface was constantly evaporating rather than recrystallizing so that the vapor from both sides could not transport to the surface powder and only deposited on the surface of the seed crystal. The gas was no longer concentrated in the graphitized area, reducing the possibility of carbon inclusions during crystal growth.

We find that the size of the graphite block directly affected the growth rate of the SiC crystal. When the size of the graphite block was too large, the SiC powder in the graphite crucible could not maintain the crystal growth process for a long time, and the growth rate of the late crystal was low. Therefore, the radius and the height of the graphite block were controlled at 35–45 mm and at 80–95 mm, respectively. The growth rate of SiC crystal after adding graphite blocks of different sizes was simulated, the results are shown in Figure 7a. When the radius was 35 mm, and the height was 80 mm, the average crystal growth rate was fastest with 280 $\mu\text{m}/\text{h}$. Figure 6b shows the growth rate at different times. By comparing the growth rates of the two structures, it was found that the growth rate of the optimized structure was firstly higher then slightly lower than that of the traditional structure before 35 h of crystal growth. The graphite blocks increase the powder sublimation rate of the surface area in the early growth stage, resulting in an increase in the growth rate. After long-time growth, with the complete sublimation of powder in the surface area, the growth rate decreases slightly.

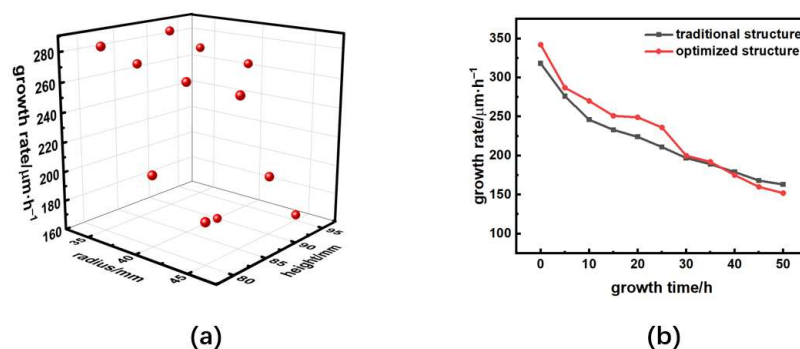


Figure 7. Crystal growth rate with different graphite block sizes: (a) average growth rate with different graphite block sizes and (b) growth rate at different time in different structure.

4. Conclusions

In this paper, we simulated the temperature distribution in the powder, the evolution of the powder, and the gas transport in different crystal growth structures. The simulation results of the traditional structure showed that the temperature difference of the powder was large. In the process of crystal growth, only the powder on both sides of the graphite crucible was sublimated. The powder at the top and bottom was recrystallized due to the low temperature. We found the utilization rate of the powder was very low in the traditional structure. Furthermore, the simulation results of the gas transport showed that there was a reverse transfer phenomenon above the powder, which caused the convection of the vapor inside the powder, and increased the possibility of inclusion of carbon inclusions during crystal growth. We proposed a new structure, which used a graphite block to replace part of the SiC powder. The high thermal conductivity of graphite improved the temperature and sublimation rate of the surface powder, resulting in the reverse transport phenomenon being eliminated. We conclude that the new structure with the graphite block inside the powder can greatly reduce the cost and improve the crystal quality.

Author Contributions: Conceptualization, H.L.; methodology, H.L.; validation, H.L., X.H.; formal analysis, H.L. and X.H.; investigation, H.L.; writing—original draft preparation, H.L.; writing—review and editing, H.L., X.H., Y.H. and X.P.; supervision, D.Y. and X.P. All authors have read and agreed to the published version of the manuscript.

Funding: This work was supported by the (1) National Key Research and Development Program of China (Grant Nos. 2017YFA0205704, 2018YFB2200101), (2) Natural Science Foundation of China (Grant Nos. 91964107, 61774133), (3) Fundamental Research Funds for the Central Universities (Grant No. 2018XZZX003-02), (4) Natural Science Foundation of China for Innovative Research Groups (Grant No. 61721005), and the (5) Zhejiang University Education Foundation Global Partnership Fund.

Institutional Review Board Statement: Not applicable.

Informed Consent Statement: Not applicable.

Data Availability Statement: Not applicable.

Conflicts of Interest: The authors declare no conflict of interest.

References

1. She, X.; Huang, A.Q.; Lucía, Ó.; Ozpineci, B. Review of silicon carbide power devices and their applications. *IEEE Trans. Ind. Electron.* **2017**, *64*, 8193–8205. [[CrossRef](#)]
2. Kimoto, T. Bulk and epitaxial growth of silicon carbide. *Prog. Cryst. Growth Charact. Mater.* **2016**, *62*, 329–351. [[CrossRef](#)]
3. Wright, N.G.; Horsfall, A.B.; Vassilevski, K. Prospects for SiC electronics and sensors. *Mater. Today* **2008**, *11*, 16–21. [[CrossRef](#)]
4. Huang, Y.C.; Wang, R.; Qian, Y.X.; Yang, D.R.; Pi, X.D. Theoretical study on the improvement of the doping efficiency of Al in 4H-SiC by co-doping group-IVB elements. *Chin. Phys. B* **2021**, in press. [[CrossRef](#)]
5. Yeo, I.G.; Yang, W.S.; Park, J.H.; Ryu, H.B.; Lee, W.J.; Shin, R.C.; Nishino, S. Two-inch a-plane (11-20) 6H-SiC crystal grown by using the PVT method from a small rectangular substrate. *J. Korean Phys. Soc.* **2011**, *52*, 1541–1544. [[CrossRef](#)]
6. Agarwal, A.; Das, M.; Krishnaswami, S.; Palmour, J.; Richmond, J.; Ryu, S.H. SiC power devices—An overview. *MRS Online Proc. Libr. (OPL)* **2004**, *815*, 243–254. [[CrossRef](#)]
7. Luo, H.; Zhang, X.Q.; Yang, D.R.; Pi, X.D. Research progress on high-purity SiC powder for single-crystal SiC growth. *J. Synth. Cryst.* **2021**, *50*, 1562–1574.
8. Wellmann, P.J.; Bickermann, M.; Hofmann, D. In situ visualization and analysis of silicon carbide physical vapor transport growth using digital X-ray imaging. *J. Cryst. Growth* **2000**, *216*, 263–272. [[CrossRef](#)]
9. Karpov, D.S.; Bord, O.V.; Karpov, S.Y.; Zhmakin, A.I.; Ramm, M.S.; Makarov, Y.N. Mass transport and powder source evolution in sublimation growth of SiC bulk crystals. *Mater. Sci. Forum* **2001**, *353*, 37–40. [[CrossRef](#)]
10. Herro, Z.G.; Wellmann, P.J.; Pusche, R.; Hundhausen, M.; Ley, L.; Maier, M.; Masri, P.; Winnacker, A. Investigation of mass transport during PVT growth of SiC by C-13 labeling of source material. *J. Cryst. Growth* **2003**, *258*, 261–267. [[CrossRef](#)]
11. Kulik, A.; Bogdanov, M.V.; Karpov, S.Y.; Ramm, M.S.; Makarov, Y.N. Theoretical analysis of the mass transport in the powder charge in long-term bulk SiC growth. *Mater. Sci. Forum* **2004**, *457*, 67–70. [[CrossRef](#)]
12. Cai, D.; Zheng, L.L.; Zhang, H.; Zhuang, D.; Herro, Z.G.; Schlessler, R.; Sitar, Z. Effect of thermal environment evolution on AlN bulk sublimation crystal growth. *J. Cryst. Growth* **2007**, *306*, 39–46. [[CrossRef](#)]

13. Wellmann, P.J.; Hofmann, D.; Kadinski, L.; Selder, M.; Straubinger, T.L.; Winnacker, A. Impact of SiC source material on temperature field and vapor transport during SiC PVT crystal growth process. *Mater. Sci. Forum* **2001**, *353*, 11–14. [[CrossRef](#)]
14. Bogdanov, M.V.; Galyukov, A.O.; Karpov, S.Y.; Kulik, A.V.; Kochugueva, S.K.; Ofengeima, D.K.; Tsiryulnikova, A.V.; Ramm, M.S.; Zhmakin, A.I.; Makarov, Y.N. Virtual reactor as a new tool for modeling and optimization of SiC bulk crystal growth. *J. Cryst. Growth* **2001**, *225*, 307–311. [[CrossRef](#)]
15. Li, H.; Chen, X.L.; Ni, D.Q.; Wu, X. Factors affecting the graphitization behavior of the powder source during seeded sublimation growth of SiC bulk crystal. *J. Cryst. Growth* **2003**, *258*, 100–105. [[CrossRef](#)]
16. Wang, X.L.; Cai, D.G.; Zhang, H. Increase of SiC sublimation growth rate by optimizing of powder packaging. *J. Cryst. Growth* **2007**, *305*, 122–132. [[CrossRef](#)]
17. Liu, X.; Chen, B.-Y.; Song, L.-X.; Shi, E.-W.; Chen, Z.-Z. The behavior of powder sublimation in the long-term PVT growth of SiC crystals. *J. Cryst. Growth* **2010**, *312*, 1486–1490. [[CrossRef](#)]
18. Geiser, J.; Klein, O.; Philip, P. Transient numerical study of temperature gradients during sublimation growth of SiC: Dependence on apparatus design. *J. Cryst. Growth* **2006**, *297*, 20–32. [[CrossRef](#)]
19. Wellmann, P.; Herro, Z.; Winnacker, A.; Püsche, R.; Hundhausen, M.; Masri, P.; Kulik, A.; Bogdanov, M.; Karpov, S.; Ramm, M. In situ visualization of SiC physical vapor transport crystal growth. *J. Synth. Cryst.* **2005**, *275*, 1807–1812. [[CrossRef](#)]
20. Yang, K.; Yang, X.L.; Cui, Y.X.; Peng, Y.; Chen, X.F.; Hu, X.B.; Xu, X.G. Carbon inclusions in silicon carbide single crystals grown by physical vapor transport method. *J. Synth. Cryst.* **2014**, *43*, 1602–1606.